nature communications

Article

https://doi.org/10.1038/s41467-026-71881-3

Probing universal phase diagram of dimensional crossover with an atomic quantum simulator

Received: 20 June 2025

Accepted: 25 March 2026

Published online: 15 April 2026

Check for updates

Jinyuan Tian[1,5], Zhongcheng Yu[1,5], Jing Liu[2,3], Chi-Kin Lai[1], Lorenzo Pizzino[4], Chengyang Wu[1], Hongmian Shui[1,3], Thierry Giamarchi[4] ✉, Hepeng Yao[1] ✉ & Xiaoji Zhou[1,3] ✉

Dimensionality is a fundamental concept in physics, which plays a hidden but crucial role in various domains, including condensed matter physics, relativity and string theory, statistical physics, etc. In quantum physics, reducing dimensionality usually enhances fluctuations and leads to novel properties. Owing to these effects, quantum simulators in which dimensionality can be controlled have emerged as a new area of interest. However, such a platform has only been studied in specific regimes and a universal phase diagram is lacking. Here, we produce an interacting atomic quantum simulator with continuous tunability of anisotropy and temperature, and probe the universal phase diagram of dimensional crossover. At low temperatures, we identify the regimes from quantum three to zero dimensions. By increasing temperature, we observe the non-trivial emergence of a thermal regime situated between the quantum zero and integer dimensions. We show that the quantum-to-thermal transition falls into four different universality classes depending on the dimensionality. Surprisingly, we also detect a fifth type where the high-dimensional quantum system can reach the thermal phase by crossing a low-dimensional quantum regime. Our results provide a crucial foundation for understanding the projective condensed matter structures in unconventional dimensions.

The Euclidian space we live in is three-dimensional (3D), where the equations of states or motions are well defined and studied. In recent years, research objects with dimensionality different from three are widely found naturally or artificially. They usually lead to novel physical properties, quite different from the ones of the 3D world. For instance, relativity and string theory, which plays an important role in particle physics and cosmology, mostly rely on dimensions larger than three[1]. In condensed matter physics, fractal structures can play an important role. They are usually characterized by the so-called fractal dimension, which is non-integer[2,3].

In microscopic physics, be it classical or quantum, the role of dimensionality is also essential. Even for a classical system which can be described by the Boltzmann distribution, the probability density function of kinetic energy exhibits totally different dependence between three and low dimensions[4]. In quantum physics, the distinction is even stronger owing to the very different properties of quantum fluctuation in different dimensions. Various types of high-temperature

[1]State Key Laboratory of Photonics and Communications, School of Electronics, Peking University, Beijing, China. [2]Institute of Advanced Functional Materials and Devices, Shanxi University, Taiyuan, Shanxi, China. [3]Institute of Carbon-based Thin Film Electronics, Peking University, Taiyuan, Shanxi, China. [4]DQMP, University of Geneva, Geneva, Switzerland. [5]These authors contributed equally: Jinyuan Tian, Zhongcheng Yu. ✉e-mail: thierry.giamarchi@unige.ch; hepeng.yao@pku.edu.cn; xjzhou@pku.edu.cn

and organic superconductors show novel properties arising from reduced dimensionality[5–7]. However, controlling parameters like the tunneling rates along different directions (e.g. with pressure or chemistry) accurately and continuously, remains challenging[8,9]. Therefore, the atomic quantum simulators, mainly realized by ultracold atoms in optical potentials, has been widely extended to low dimensional structures in recent years owing to high controllability[10–12]. In one or two dimensions, they reveal remarkable phenomena, such as the fermionization of bosons[13,14], Tomonaga-Luttinger Liquid (TLL)[15] type of correlation, topological properties[16,17], frustrated phase[18] and the Berezinskii-Kosterlitz-Thouless (BKT) transition[19,20]. Although most systems are firmly based in one of the integer dimensions, some systems can, as a function of parameters, show behavior pertaining to several dimensionalities, known as dimensional crossover. In recent experiments, this phenomenon was analyzed using quantum simulators based on atomic[21–24] and photonic systems[25] in certain regimes. In these simulators, special behaviors of superfluidity and quantum correlation are observed, which reflect properties of multiple dimensions.

Temperature and interaction are two important parameters for the dimensional crossover of the quantum simulators. At zero temperature, the mechanism is clear[10,26]. For a quantum system at dimension D, providing a constraint on D' directions will suppress the tunneling rate along them and produce a system with dimensionality $D - D'$, see the sketch in Fig. 1a1, b1. Moving to finite temperature with zero interactions, temperature will simply provoke dimensional crossover when it coincides with the kinetic energy in the transverse directions D'. However, the mechanism with both finite temperature and interactions is non-trivial, since the tunneling between the blocks is not of the free-particle type any more. Previous works have only carried out studies for such a system in specific regimes or for specific quantities, theoretically[15,27–31] and experimentally[21–23,32–35]. However, a study that reflects the universal properties of dimensional crossover for such a quantum simulator is lacking. Especially, the universal nature of the finite-temperature phase diagram for an interacting system is not clear.

In this work, we provide the first probe of the universal phase diagram of dimensional crossover with an atomic quantum simulator. Loading ultracold atomic systems into triangular optical lattices, we obtain an interacting simulator with high tunability of anisotropy and temperature. At tens of nano-Kelvin, we can identify quantum regimes at different dimensionalities. By measuring the detailed phase diagram at different temperatures, two important universal features appear, see Fig. 1b2. On the one hand, for each fixed temperature, the thermal (TH, classical) regime always appears between 0D and positive integer-D quantum regimes, which can be explained by the interplay of quantum and thermal fluctuations. On the other hand, by increasing temperature for fixed anisotropy, we find the quantum-to-thermal transitions falling into different universality classes for different dimensionalities, namely the BEC transition (3D), BKT transition (2D), TLL transition (1D) and melting effect of Mott insulator (0D) accordingly. Strikingly, we also detect a fifth type of transition different from these four. For some special cases, the quantum 3D system can reach the thermal state via a low-dimensional quantum phase, instead of a direct transition. This suggests that, by increasing temperature, a dimensional crossover between quantum systems may happen before the thermal transition. Our experimental data are in good agreement with quantum Monte Carlo.

Results

Our experiment starts from a Rb-87 Bose-Einstein Condensate (BEC) in the hyperfine state $F = 1$ trapped in a crossed optical dipole trap containing typically 2.5×10^5 atoms[36], see Fig. 1a1. Its 3D s-wave scattering length is $a_{3D} = 107(4)a_0$. We can control the system's temperature from 16 nK up to 455 nK without significantly altering the atom number by adjusting both the MOT loading time t_{MOT} before evaporative cooling and the final optical intensity (equivalently higher final trapping frequency $\bar{\omega}$) at the end of evaporative cooling, under a properly chosen function $t_{MOT}(\bar{\omega})$ (See Supplementary Fig. 2). Then, we adiabatically ramp up a 3D optical lattice with lattice spacing $a = \lambda/2 = 532$ nm in 80 ms and hold it for 20 ms. As shown in Fig. 1a1, our optical lattices consist of a 2D triangular lattice (x-y plane, blue arrows) parallel to the direction of gravity (y direction) and a 1D lattice (z direction, green arrows) perpendicular to it. The laser beams for the 1D and 2D lattices have a frequency difference of 110 MHz to ensure no interference between their laser beams. The lattice depths of the 2D triangular lattice V_{2D} and the 1D constrained lattice V_{1D} range from 0 to 25 E_r and 0 to 70 E_r, respectively, with an accuracy of 0.2%, where $E_r = \pi^2\hbar^2/(2ma^2)$ is the recoil energy, with $\hbar$ the reduced Planck's constant and m the mass of particles.

The experimental sequence starts from preparing the BEC at the targeted temperature. Then, we independently tune the depths of the

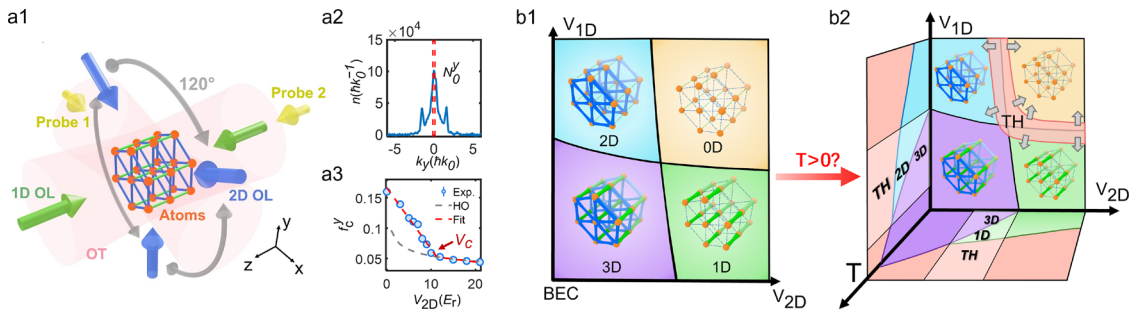

Fig. 1 | Illustration of the experiment. a1 Sketch of the BEC system loading into a laser potential consisting of crossover optical dipole trap (OT, red cylinders), 1D optical lattice (1D OL, green arrows, z direction) and 2D triangular optical lattices (OL, blue arrows, x-y plane). The gravity is along the y-direction, while 1D lattice is aligned along the z-direction. The yellow arrows show the two probes. **a**2 The momentum distribution from the TOF images for the case with lattice depths $V_{2D} = 5.0E_r$ and $V_{1D} = 0.0E_r$, and temperature $T = 23$nK. The red dashed lines mark the zero-momentum area, which contains N_0^y atoms. **a**3 The typical behavior of f_c^y (blue circles) as a function of V_{2D} with the same T and V_{1D} as (**a**2). The red dashed line is the piecewise fit, which decides the critical potential V_c. The gray dashed line is f_c^y computed by harmonic trap approximation. **b**1 The sketch for the phase diagram of dimensional crossover at zero temperature, where the quantum 3D (purple), 2D (blue), 1D (green) and 0D (yellow) regimes are presented. In each phase, the subplot depicts the structural diagram, where lattice sites (orange sphere) are connected by coupling (blue and green lines), be it coherent(solid) or incoherent(dashed). **b**2 The sketch for the finite-temperature behavior observed in this work. For fixed temperature, we find a thermal phase (TH) appears between zero and positive dimensions. When increasing temperature for fixed anisotropy, we find four common quantum-to-thermal transitions and one special type, where the system reaches the thermal phase via low-dimensional quantum regimes, such as 3D-1D-TH.

https://doi.org/10.1038/s41467-026-71881-3

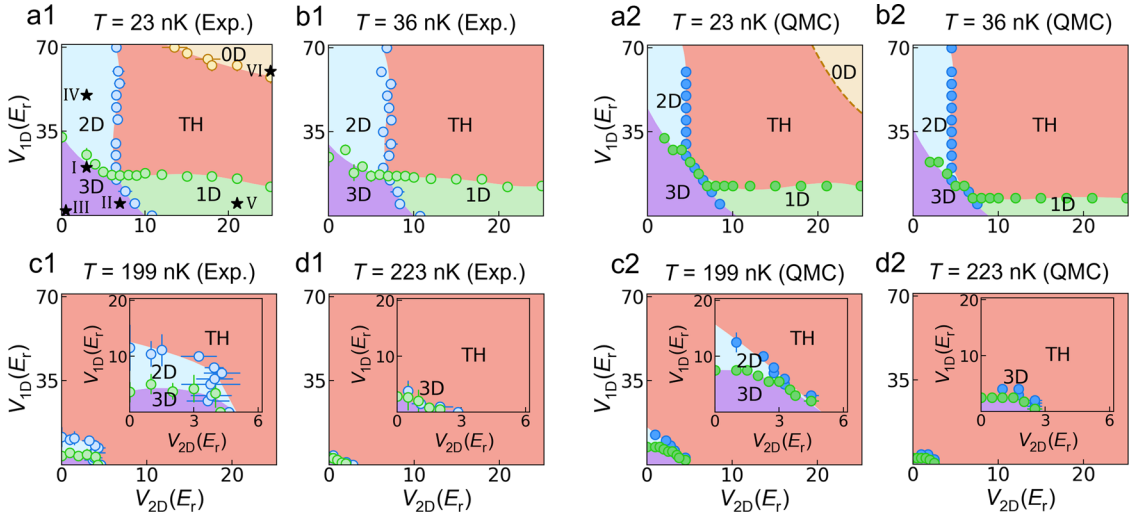

Fig. 2 | The universal phase diagram of dimensional crossover at different temperatures. a1–4 are the experimentally measured phase diagrams at initial BEC temperatures T = 23(5), 36(3), 199(25) and 223(29) nK, as a function of the lattice amplitudes V_{2D} and V_{1D}. Here, we observe quantum regimes at 3D (purple), 2D (blue), 1D (green), 0D (yellow) as well as the thermal regime (TH, red). The transition points are judged by zero-momentum fraction (blue and green circles) and correlation function (yellow circles). Insets in (**c**1) and (**d**1) are a zoom around the low-lattice-depth area. Error bars are obtained from the piecewise fit as in Fig. 1a3. The experimental parameters are particle number $N = 2.5(3) \times 10^5$ and 3D s-wave scattering length $a_{3D} = 107(4)a_0$ with trap frequencies $(\omega_x, \omega_y, \omega_z)/2\pi$ ranging from (27,84,80) Hz to (60,135,121) Hz depending on the temperature considered. (**a**2)–(**d**2) are the counterpart for (**a**1)–(**d**1), which present the QMC simulations for equivalent homogeneous systems.

2D triangular and 1D lattices to tune the anisotropy of the system. After holding it for another 20 ms, we make sure the system reaches an equilibrium state[37]. Next, we remove both the optical dipole traps and lattices for 28 ms time-of-flight (TOF) and take the absorption image. With the images from the two probes along the x and z directions (yellow arrows in Fig. 1a1), we observe the momentum distribution from which we extract useful information. More specifically, as suggested by refs. 23,29,30,38, we access the zero-momentum fraction along a certain direction. For instance, for the y direction, it is defined as

$$f_c^y = \frac{\int_{-\infty}^{+\infty} dk_x \int_{-\infty}^{+\infty} dk_z \int_{-\Delta k_y}^{+\Delta k_y} n(\mathbf{k}) dk_y}{\int_{-\infty}^{+\infty} dk_x \int_{-\infty}^{+\infty} dk_z \int_{-\infty}^{+\infty} n(\mathbf{k}) dk_y}, \tag{1}$$

with $n(\mathbf{k})$ the momentum distribution, $\Delta k_y = 2\pi/L_y$ the zero-momentum width and L_y the system size. Such a quantity reflects the quantum coherence properties along certain directions. It is more accurate than the visibility of the momentum diffraction peak[39] and has been proved to be efficient for studying the dimensional crossover[23,29,30]. Notably, this quantity is a vector and different from the scalar condensate fraction.

From the typical momentum distribution as in Fig. 1a2, we compute the f_c^y and construct Fig. 1a3. Clearly, we can apply fit of a piecewise linear function (dashed red line)

$$f_c(V) = \begin{cases} -k_1 V + f_{c0} & (V < V_c), \\ -k_2 V_c - k_1 V + f_{c0} & (V > V_c), \end{cases} \tag{2}$$

where all of the k_1, k_2, f_{c0} and V_c are fitting parameters. From this, we determine the critical lattice depth V_c (See Supplementary Fig. 3). This method has been proven effective in previous works[23,29,30]. Especially, for low-dimensional systems at low temperatures, one always finds that transverse f_c^i in the large enough potential regime fits nicely with that of the ground state of a harmonic oscillator (dashed gray line).

At zero temperature, the physics of such a system is qualitatively clear, see Fig. 1b1. When both V_{2D} and V_{1D} are small, the system is a 3D BEC with modulated density. When increasing V_{1D} (V_{2D} resp.) while keeping V_{2D} (V_{1D} resp.) small, the coupling along the z direction (x, y directions resp.) becomes incoherent, while it remains coherent along the others. This is the regime of the 2D (1D resp.) atomic quantum simulator. In the limit where both V_{2D} and V_{1D} are large, the system effectively becomes 0D. All sites are decoupled due to quantum fluctuations and this is equivalent to the 3D Mott-insulator regime observed in refs. 37. However, as mentioned above, the interacting systems at finite temperatures remain unclear and form the central focus.

We first prepare our interacting BEC at different values of initial finite temperature T and measure the phase diagram as a function of V_{2D} and V_{1D}, see Fig. 2 for four typical cases. The blue and green circles are the critical lattice depths along the two directions, respectively, judged by f_c^y and f_c^z. Notably, we benefit from the use of a triangular lattice, which allows us to more easily tune the effective dimension of the system (Supplementary Fig. 1). Here, we always load the lattice adiabatically and thus each diagram is isentropic. At the lowest temperature we realized, i.e., 23 nK, we find the four quantum regimes at different dimensionalities as predicted in Fig. 1b1. To further locate the thermal regime, we scan the zero-momentum fraction and correlation length as a function of T for a large scale of data points, and check when these quantities saturate at a small value (yellow circles, see details below). Interestingly, we find the thermal regime appears to be located between the zero- and positive integer dimensional quantum regimes. This behavior can be explained by the different effects of thermal fluctuations. For the 0D system, it is an incompressible insulator with finite gaps whose correlation length is independent of temperature. The quantum-to-thermal transition for such a system is the melting of the gap[40,41], leading to a compressible thermal phase with a T-dependent correlation length. Thus, systems with a smaller gap, i.e., smaller lattice amplitude, will be melted first. On the other hand, for quantum systems at positive integer dimensionalities, the quantum-to-thermal transition is induced by the joint contribution of quantum and thermal fluctuations. When the effective dimensionality is larger, i.e., smaller lattice amplitude, the quantum fluctuation is smaller and it calls for a higher temperature to enter the thermal

https://doi.org/10.1038/s41467-026-71881-3

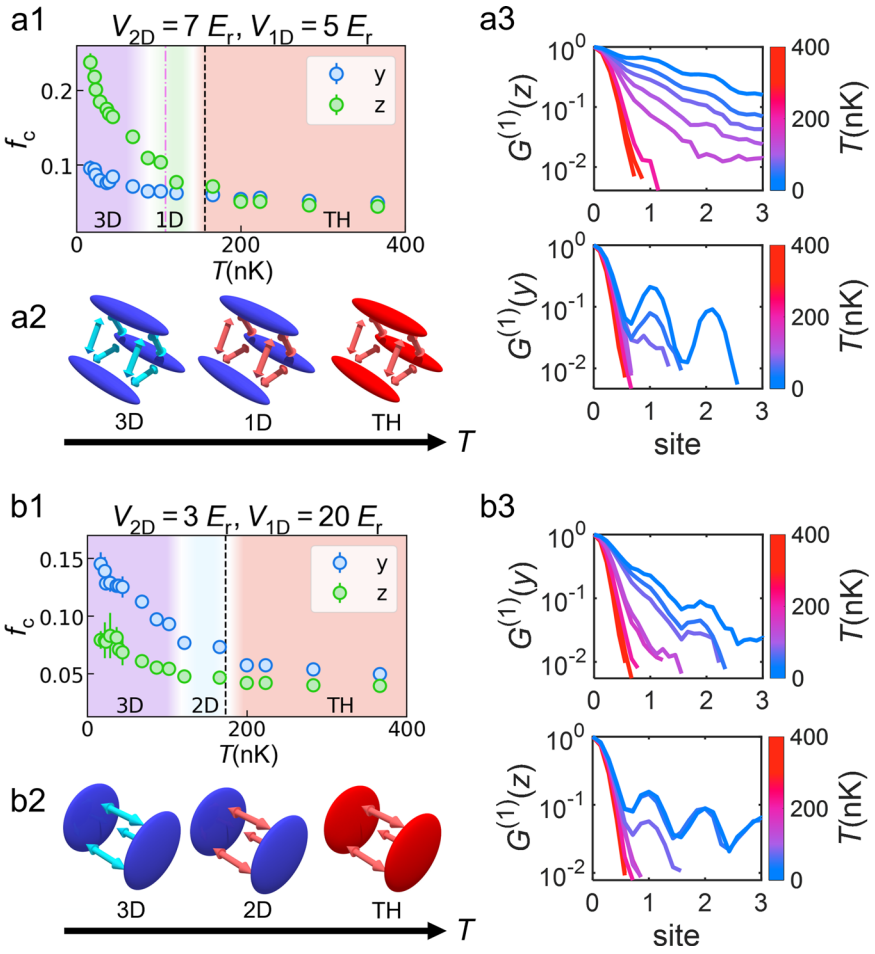

Fig. 3 | Special category of finite temperature transition. We show the zero-momentum fraction along two directions f_c^y (blue circles) and f_c^z (green circles) as a function of temperature T, for two different cases: **a**1 $V_{2D} = 3.0E_r$, $V_{1D} = 20.0E_r$ and **b**1 $V_{2D} = 7.0E_r$, $V_{1D} = 5.0E_r$. Error bars represent the standard deviation of five measurements. The colored areas represent the judged regimes. The white region is the estimated transition temperature from piecewise fit of experimental data and its width represents the errorbars. **a**2 and **b**2 are illustration for the physical pictures, where blue (red resp.) layers or tubes indicate quantum (thermal resp.) gases. Light blue (red resp.) legs indicate coherent (incoherent resp.) coupling. **a**3 and **b**3 are the corresponding correlation function $G^{(1)}$ along y and z directions at different temperatures. Experimental parameters: particle number $N = 2.5(3) \times 10^5$ and 3D s-wave scattering length $a_{3D} = 107(4)a_0$.

phase[10–12,42]. Thanks to the two processes mentioned above, the thermal phase appears in the middle of the phase diagram as in Fig. 2a1. As the temperature increases, the quantum regimes shrink successively and the thermal regime expands, see Fig. 2a1–d1. We find that the 0D, 1D, 2D, 3D quantum regimes disappear at the temperature of $T = 36$ nK (b1), 199 nK (c1), 223 nK (d1) and 250 nK, correspondingly. This fits with our previous statement.

To further confirm our observations, we run QMC simulations of an equivalent homogeneous system (see details in Method) and generate the phase diagram by studying the superfluid stiffness, see Fig. 2a2–d2. Although the superfluid stiffness does not necessarily equal to the zero-momentum fraction, they both reflect the quantum coherence properties along certain directions and both of them have been proved to be efficient indicators for identifying the critical points of dimensional crossover, see discussions in refs. 28–30. From the QMC phase diagrams Fig. 2a2–d2, we qualitatively recover the same experimental phase diagrams. The quantitative discrepancy might be due to different factors, such as the presence of the harmonic trap and the variation of the number of particles. Notably, according to the QMC simulations, increasing the atom number, changing the system lengths and adding the presence of the harmonic trap do not qualitatively change the results, but only affect the regions of different phases quantitatively (Supplementary Figs. 4–8).

In order to further study the properties of the quantum-to-thermal transition, we now choose six typical points (I-VI) in Fig. 2a1, and scan f_c^y and f_c^z as a function of temperature T while maintaining the particle numbers N almost unchanged. The results are shown in Figs. 3 and 4. Notably, here we use f_c^y to study the coherence properties in the 2D xy – plane thanks to the rotational symmetry of the triangular lattices (See Supplementary Fig. 11).

Although most of the cases fall into typical universality classes of quantum-to-thermal phase transition, there are some special points which show strikingly different behaviors, for instance points I and II in Fig. 2a1. Their finite temperature properties are shown in Fig. 3. In Fig. 3a1, we consider the lattice depth as point I and scan temperature. Interestingly, we find that f_c^y and f_c^z drop to a plateau at different values of temperature, namely $T_1 = 88 \pm 28$nK and $T_2 = 142 \pm 14$nK (white lines). This suggests, instead of a direct transition from 3D quantum to thermal phase, an intermediate 1D quantum regime emerges in between. It can be viewed as thermal fluctuation-induced dimensional crossover, such that we name it "TFDC" type. Similar behavior has also been observed for another anisotropy case where V_{1D} is large, see Fig. 3b1. The two f_c drop to the plateau at two different temperatures, namely $T_1 = 119 \pm 19$nK and $T_2 = 177 \pm 20$nK (white lines). Similarly, it suggests a 3D-2D-TH process. For both of the two cases, we evaluated the difference between the two critical temperatures using a statistical

https://doi.org/10.1038/s41467-026-71881-3

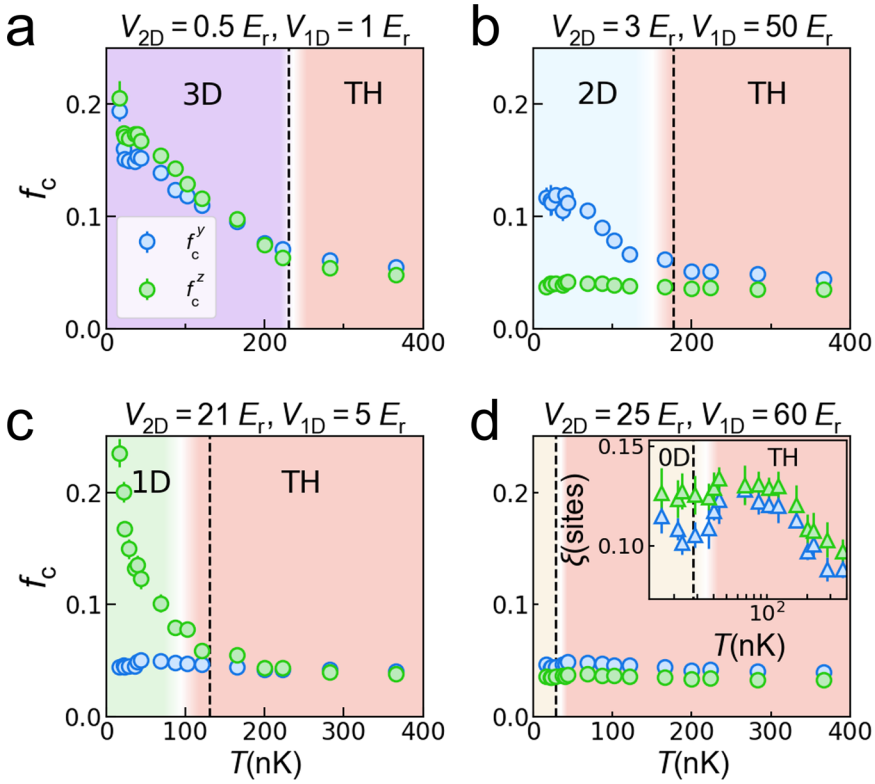

Fig. 4 | The common quantum-to-thermal transition for different integer dimensionalites. The behavior of zero-momentum fraction f_c along the y (blue) and z (green) directions as a function of temperature T. At the lowest temperature, the system is a quantum gas in the 3D (**a** $V_{2D} = 0.5E_r$, $V_{1D} = 1E_r$), 2D (**b** $V_{2D} = 3.0E_r$, $V_{1D} = 50.0E_r$), 1D (**c** $V_{2D} = 21.0E_r$, $V_{1D} = 5.0E_r$) and 0D (**d** $V_{2D} = 25.0E_r$, $V_{1D} = 60.0E_r$) regimes, respectively. Error bars represent the standard deviation of five measurements. The white region is the estimated transition temperature from the experimental data and the dashed lines are theoretical predictions. The inset of (**d**) shows the correlation length ξ as a function of T. Experimental parameters: particle number $N = 2.5(3) \times 10^5$ and 3D s-wave scattering length $a_{3D} = 107(4)a_0$.

significance test. The null hypothesis of equality was rejected with a p-value of 0.035, indicating a statistically significant difference. (See Supplementary Figs. 9, 10)

In principle, the TFDC process crosses the same dimensional crossover line as those in refs. 23,31,33–35. However, it goes through the crossover line via the temperature axis, which is different from the previous work. Notably, to probe these behaviors along temperature axis, one always has a certain anisotropy i.e., lattice amplitudes along directions j and j' have a certain ratio. How should we understand it? As suggested by theoretical works[27,29,30], the temperature competes with the effective hopping amplitude, renormalized by the interaction, leading to the dimensional crossover. When it reaches the smaller hopping amplitude t_j, the particles are driven by thermal fluctuations along that direction. Effectively, we have one less direction where the system behaves coherently, see illustration in Fig. 3a2, b2. Therefore, as long as it happens below the thermal transition temperature, increasing temperature only eliminates the quantum coherence along j direction but not the others like j'. This leads to a crossover from 3D quantum system to thermal regime via a low-D quantum phase.

Notably, in order to probe these behaviors, one always needs to carefully pick up a point nearby the crossover line between the 3D and low-D regimes at low temperature, such that the temperature of dimensional crossover is much lower than the one to thermal phase. Although such mechanism was proposed in condensed matter systems[6,7], detecting it precisely is challenging given the difficulty in controlling the anisotropy accurately. Thanks to the high tunability of parameters in our triangular lattice platform, we provide the first controlled test of this phenomenon.

To further confirm our demonstration, we perform two additional analysis. First, we estimate the 3D-1D crossover temperature via field theory[30]. By treating the system as coupled quantu m chains, we can perform a mean-field (MF) decoupling to estimate the crossover temperature[27,30]

$$T_{3-1D} = A_B t_\perp^{-\nu}, \tag{3}$$

with $\nu = \frac{2K}{4K-1}$ the scaling exponent and K the Luttinger parameter encoding the effect of interactions. A_B is the prefactor which depends on Luttinger parameters K, particle density n and system size L. (See Supplementary Information Section 2 for calculation of atomic density) Using the experimental parameters, we find the temperature to be $T_{3-1D} = 108$ nK (purple dashed line), which fits with T_1 within errorbars in Fig. 3a1.

Another proof is the data of the one-body correlation function $G^{(1)}(r) = \int \langle \Psi^\dagger(r)\Psi(r')\rangle dr'$, which can be computed by the Fourier transform of the measured momentum distribution. It reflects clearly the correlation decay pattern along single directions. In Fig. 3a3, we show the decay of $G^{(1)}(y)$ and $G^{(1)}(z)$ at different temperatures. Clearly, above $T_1 = 88 \pm 28$ nK, the correlation along y direction drops extremely fast (faster than 1 site) and remains unchanged for higher temperatures. On the contrary, along the z direction, the correlation drops faster while temperature increases, and only remains unchanged after $T_2 = 142 \pm 14$ nK. This further confirms the existence of the 3D-1D-TH transition at these two temperatures. In Fig. 3b3, similar behaviors are found for case II, where a signature of 3D-2D-TH transition is presented. Here, the oscillation of the correlation function originates from the periodicity of the correlation function, which will be blurred by the decay of correlation in the large potential limit. (For more details, see Supplementary Information Section 3.5.)

Now, we turn back to discuss the other common cases of the quantum-to-thermal transitions. In Fig. 2a2, cases like I and II are minority. The majority should fall into four different universality classes of phase transitions, namely the BEC transition (3D), BKT transition (2D), TLL transition (1D) and Mott melting (0D). Here, we pick up four points deeply in the regimes of 3D (III), 2D (IV), 1D (V) and 0D (VI), and study the behavior of measured f_c^y and f_c^z as a function of temperature T, see Fig. 4a–d, correspondingly.

In Fig. 4a, the system starts from a 3D BEC at low temperature. By increasing temperature, both f_c^y and f_c^z drop together and reach a plateau at an identical value of $T_{3D}^{exp} = 236 \pm 17$ nK. Here, the transition temperature for a trapped 3D BEC writes[43]

$$T_{3D} = T_{BEC} = 0.94 \frac{\hbar \bar{\omega} N^{1/3}}{k_B}, \tag{4}$$

with N the atom number, $\bar{\omega} = (\omega_x \omega_y \omega_z)^{1/3}$ the average trapping frequency of the optical dipole trap, and k_B the Boltzmann constant. It gives T_{BEC} = 230nK (black dashed line) with our experimental parameters and fits nicely with our measured T_{3D}^{exp} within 2.6%.

For the 2D case, f_c^z is always very small regardless of the value of temperature, while f_c^y drops at $T_{2D}^{exp} = 151 \pm 23$ nK and then remains constant, see Fig. 4b. This transition should be captured by the BKT transition class, whose transition temperature can be computed as[44,45]

$$n_{2D} \lambda_{T_{2D}}^2 = ln(\xi/4\pi) + lnln(1/n_{2D} a_{2D}^2), \tag{5}$$

where n_{2D} is the 2D density, $\lambda_T = \sqrt{h^2/2\pi m k_B T}$ is the thermal de Broglie wavelength, a_{2D} is the 2D scattering length. The numerical coefficient $\xi = 380$ is calculated in ref. 44. Here, we find $T_{BKT} = 176.3$ nK (black dashed line), which fits with the observed temperature T_{2D}^{exp} within 15.5%. Notably, for the case in Fig. 3b1, we can also estimate the 2D-TH transition temperature with Eq. (5). It gives $T_{2D} = 172.6$ nK (black dashed line), which fits nicely with the experimental observation within 2.5%.

For the 1D case, while temperature increases, we find f_c^y remains a small constant while f_c^z decreases up to $T_{1D}^{exp} = 95 \pm 23$ nK, see Fig. 4c. This transition can be captured by the Tomonaga-Luttinger liquid theory[15,46]. Specifically, its transition temperature writes

$$\xi(T = T_{1D}) = \frac{3\hbar^2 \bar{n}_{1D}}{2 m k_B T_{1D}} \ll L, \tag{6}$$

with ξ the correlation length, n_{1D} the 1D density and L the system size. In practice, we take $\xi(T = T_{1D}) = L/10$ and it predicts $T_{1D} = 130.9$nK (black dashed line), which fits with our observation within 31.8%. Similarly, we can apply this to the 1D-TH transition in Fig. 3(a1). It gives $T_{1D} = 155.5$nK (black dashed line), which fits with our observation within 8.7%.

The finite temperature effect for a 0D quantum system corresponds to the melting effect discussed above. Both f_c^y and f_c^z are small at low temperature and remain almost unchanged with temperature, see Fig. 4d. To further capture this melting effect, we obtain the correlation function $G^{(1)}(x)$ from the measured $n(\mathbf{k})$, and by performing an exponential fit $G^{(1)}(x) \sim e^{-|x|/\xi}$, we extract the correlation length ξ. The temperature dependence of ξ is shown in the inset. At low temperature, it exhibits a plateau. Above the melting temperature $T_{0D}^{exp} = 35 \pm 8$ nK, it increases with temperature first, reaches a maximum value and then decreases. We argue that this stems from the competition between the increasing mobility of particles induced by particle-hole pair excitations, and the increasing thermal fluctuations. The scale of the melting temperature writes[47]

$$T_{0D} = T_{melt} \sim \frac{\Delta}{k_B}, \tag{7}$$

with Δ the Mott gap. Taking the parameters of our lattices, we find $\Delta = 57$ nK. In practice, we take $T_{melt} = 0.4\Delta/k_B = 28$ nK and find good agreement with experiment in both Figs. 2 and 4d.

Notably, in principle, the TFDC process should be different from the other quantum-to-thermal transitions, although they are both obtained by changing temperature with fixed anisotropy. The physical process of TFDC should rather be in the same class as the dimensional crossover for fixed temperatures discussed in Fig. 2[27–30], since both of them are caused by the joint effect of the potential barrier and temperature, which kills the coherent coupling along certain directions.

Discussion

Summarizing, we probe the universal phase diagram of dimensional crossover for a quantum simulator at various temperatures, using interacting ultracold atoms in 3D anisotropic optical lattices. At various temperatures, we find quantum systems at different integer dimensionalities with a thermal phase existing in between. Furthermore, we study the quantum-to-thermal transition for systems with fixed anisotropy. Five categories of transitions are identified. Especially, we provide the first controlled test of the TFDC type, benefiting from the high tunability of both temperature and anisotropy in our triangular lattice setup. Our result provides an important basis for quantum simulators with unconventional dimensionalities. Given such a platform, one can potentially carry out various further detailed tests, such as the χ^2 test for identifying the correlation decay properties for coupled low-dimensional systems[23] and what is the mixed dimensional properties at various temperatures. This kind of test also paves the way for the understanding of their projective structures in condensed matter systems, especially the organic conductors and high-temperature superconductors.

Methods

Control of temperature

Our experiment starts from a Rubidium-87 Bose-Einstein Condensate (BEC) with a typical atom number of $2.5(3) \times 10^5$ in the hyperfine state $|F = 1, m_F = -1\rangle$, as shown in Fig. 1. To further control the temperature of the produced BEC, we adjust the parameters of the evaporative cooling sequence as well as the initial state before this process. On the one hand, we prepare systems with different atom numbers before the evaporative cooling. This can be achieved by adjusting the magneto-optical trap (MOT) loading time prior to the evaporative cooling. On the other hand, we control the evaporative cooling sequence by varying both the decreasing rate and the final laser intensity. Combining these two processes properly, we can reach different temperatures while maintaining the same final atom number within a 15% difference. In our measurement, the temperature of the BEC can be adjusted between 23 nK and 455 nK, as inferred from the TOF images using bimodal fitting[36].

The optical lattice potential

Here, we clarify the details about the 1D and 2D lattice potentials. In the 2D xy-plane, our triangular lattice is formed by three traveling beams that intersect at an enclosing angle of 120°, with their linear polarization perpendicular to the 2D plane. The generated triangular lattice potential in the xy-plane is given by[32]:

$$\begin{aligned} V(x,y) &= -|E_1 + E_2 + E_3|^2 \\ &= -|\tfrac{\sqrt{V_{2D}}}{2} e^{-i\mathbf{k}_1\cdot\mathbf{r}} + \tfrac{\sqrt{V_{2D}}}{2} e^{-i\mathbf{k}_2\cdot\mathbf{r}} + \tfrac{\sqrt{V_{2D}}}{2} e^{-i\mathbf{k}_3\cdot\mathbf{r}}|^2 \\ &= -\tfrac{V_{2D}}{4}\big(3 + 2\cos((\mathbf{k}_1 - \mathbf{k}_2)\cdot\mathbf{r}) \\ &\quad + 2\cos((\mathbf{k}_2 - \mathbf{k}_3)\cdot\mathbf{r}) + 2\cos((\mathbf{k}_3 - \mathbf{k}_1)\cdot\mathbf{r})\big) \\ &= -\tfrac{V_{2D}}{4}(3 + 2\cos(k_0\sqrt{3}x) + 4\cos(k_0\tfrac{\sqrt{3}}{2}x)\cos(k_0\tfrac{3}{2}y)), \end{aligned} \tag{8}$$

where V_{2D} is the lattice depth of the 2D triangular lattice, k_1,k_2,k_3 are the wave vectors of three lattice beams. In our experiment, we always

have $\mathbf{k}_1 = \frac{2\pi}{\lambda}(\frac{\sqrt{3}}{2}, -\frac{1}{2})$, $\mathbf{k}_2 = \frac{2\pi}{\lambda}(-\frac{\sqrt{3}}{2}, -\frac{1}{2})$, $\mathbf{k}_3 = \frac{2\pi}{\lambda}(0, 1)$, and $|\mathbf{k}_1| = |\mathbf{k}_2| = |\mathbf{k}_3| = k_0$. Along the z-direction, we also load a 1D optical lattice formed by a 1064 nm standing wave light. This potential can be expressed as $V(z) = V_{1D}\cos^2(k_0 z)$, where V_{1D} is lattice depth of 1D lattice, and $k_0 = \frac{2\pi}{\lambda}$ the wave vector with $\lambda = 1064$ nm the laser wavelength.

The quantum Monte Carlo calculations

Using the quantum Monte Carlo method with worm algorithm[48,49], we simulate our experimental system based on the Bose-Hubbard model description at finite temperatures. Taking different temperature T, chemical potential μ, on-site interaction U, and tunneling $t_{x,y,z}$ along three directions, we calculate the superfluid fraction along $i-$direction $f_s^i = \rho_s^i/\rho$ $(i = x, y, j)$ by:

$$f_s^i = \frac{m}{\hbar^2}\frac{\langle W_i^2\rangle L_i^{2-d}}{\rho d\beta}, \tag{9}$$

where W_i is the winding number along i direction, L_i is the corresponding system size, d is the total dimensionality of the simulation and $\beta = 1/k_B T$ is the inverse temperature. For generating the phase diagrams in the main text (Fig. 2a2–d2), we compute the superfluid fraction f_s as a function of lattice depth V and temperature T. Typically, we perform 10^5 iterations with 10^6 warmup steps in advance, in order to make sure the Monte Carlo statistics is sufficient. The error bars of the QMC data originate from the statistical fluctuations of the sampling. Then, we determine the transition point as discussed in Figs. 1a3 and 4. In practice, we define the criterion $f_s < 0.1\%$[29]. The numerical calculations make use of the Algorithms and Libraries for Physics Simulations (ALPS) scheduler library and statistical analysis tools[50–52].

Data availability

The data of all figures shown in this manuscript and Supplementary Information are available via Zenodo[53]. All other data supporting the findings of this study are available from the corresponding author on request.

References

1. Wald, R. M. General relativity (University of Chicago Press, Chicago, 2010).
2. Akkermans, E. Statistical mechanics and quantum fields on fractals. *Contemp. Math.* **601**, 1 (2013).
3. Jagannathan, A. The Fibonacci quasicrystal: case study of hidden dimensions and multifractality. *Rev. Mod. Phys.* **93**, 045001 (2021).
4. Pathria, R. & Beale, P. D. Statistical mechanics (fourth edition) (Academic Press, London, 2021).
5. Orenstein, J. & Millis, A. J. Advances in the physics of high-temperature superconductivity. *Science* **288**, 468–474 (2000).
6. Giamarchi, T. Theoretical framework for quasi-one dimensional systems. *Chem. Rev.* **104**, 5037–5056 (2004).
7. Jerome, D. & Bourbonnais, C. Quasi one-dimensional organic conductors: from Fröhlich conductivity and Peierls insulating state to magnetically-mediated superconductivity, a retrospective. *Comptes Rendus. Phys.* **25**, 17–178 (2024).
8. Eremets, M. I. High pressure experimental methods (Oxford University Press, Oxford, 1996).
9. Dressel, M., Petukhov, K., Salameh, B., Zornoza, P. & Giamarchi, T. Scaling behavior of the longitudinal and transverse transport in quasi-one-dimensional organic conductors. *Phys. Rev. B* **71**, 075104 (2005).
10. Bloch, I., Dalibard, J. & Zwerger, W. Many-body physics with ultracold gases. *Rev. Mod. Phys.* **80**, 885–964 (2008).
11. Hadzibabic, Z. & Dalibard, J. Two-dimensional Bose fluids: an atomic physics perspective. *Riv. Nuovo Cim.* **34**, 389–434 (2011).
12. Cazalilla, M. A., Citro, R., Giamarchi, T., Orignac, E. & Rigol, M. One dimensional bosons: from condensed matter systems to ultracold gases. *Rev. Mod. Phys.* **83**, 1405–1466 (2011).
13. Paredes, B. et al. Tonks-Girardeau gas of ultracold atoms in an optical lattice. *Nature* **429**, 277 (2004).
14. Kinoshita, T., Wenger, T. & Weiss, D. S. Observation of a one-dimensional Tonks-Girardeau gas. *Science* **305**, 1125–1128 (2004).
15. Giamarchi, T. *Quantum Physics in One Dimension*, vol. 121 of *International Series of Monographs on Physics* (Oxford University Press, 2004).
16. Goldman, N. et al. Direct imaging of topological edge states in cold-atom systems. *Proc. Natl. Acad. Sci. USA* **110**, 6736–6741 (2013).
17. Tarnowski, M. et al. Measuring topology from dynamics by obtaining the Chern number from a linking number. *Nat. Commun.* **10**, 1728 (2019).
18. Struck, J. et al. Quantum simulation of frustrated classical magnetism in triangular optical lattices. *Science* **333**, 996–999 (2011).
19. Hadzibabic, Z., Krüger, P., Cheneau, M., Battelier, B. & Dalibard, J. Berezinskii–Kosterlitz–Thouless crossover in a trapped atomic gas. *Nature* **441**, 1118–1121 (2006).
20. Ha, L.C. et al. Strongly interacting two-dimensional Bose gases. *Phys. Rev. Lett.* **110**, 145302 (2013).
21. Chauveau, G. et al. Superfluid fraction in an interacting spatially modulated Bose-Einstein condensate. *Phys. Rev. Lett.* **130**, 226003 (2023).
22. Tao, J., Zhao, M. & Spielman, I. B. Observation of anisotropic superfluid density in an artificial crystal. *Phys. Rev. Lett.* **131**, 163401 (2023).
23. Guo, Y. et al. Observation of the 2D–1D crossover in strongly interacting ultracold bosons. *Nat. Phys.* **20**, 934–938 (2024).
24. Biagioni, G. et al. Dimensional crossover in the superfluid-supersolid quantum phase transition. *Phys. Rev. X* **12**, 021019 (2022).
25. Karkihalli Umesh, K. et al. Dimensional crossover in a quantum gas of light. *Nat. Phys.* **20**, 1810–1815 (2024).
26. Ho, A., Cazalilla, M. & Giamarchi, T. Deconfinement in a 2D optical lattice of coupled 1D boson systems. *Phys. Rev. Lett.* **92**, 130405 (2004).
27. Cazalilla, M. A., Ho, A. F. & Giamarchi, T. Interacting Bose gases in quasi-one-dimensional optical lattices. *N. J. Phys.* **8**, 158 (2006).
28. Bollmark, G., Laflorencie, N. & Kantian, A. Dimensional crossover and phase transitions in coupled chains: Density matrix renormalization group results. *Phys. Rev. B* **102**, 195145 (2020).
29. Yao, H., Pizzino, L. & Giamarchi, T. Strongly-interacting bosons at 2D-1D dimensional crossover. *SciPost Phys.* **15**, 050 (2023).
30. Pizzino, L., Yao, H. & Giamarchi, T. Finite size analysis for interacting bosons at the one-two dimensional crossover. *Phys. Rev. Res.* **7**, 013021 (2025).
31. Benfatto, L., Castellani, C. & Giamarchi, T. Kosterlitz-Thouless behavior in layered superconductors: the role of the vortex core energy. *Phys. Rev. Lett.* **98**, 117008 (2007).
32. Jin, S. et al. Finite temperature phase transition in a cross-dimensional triangular lattice. *N. J. Phys.* **21**, 073015 (2019).
33. Vogler, A. et al. Dimensional phase transition from an array of 1D Luttinger liquids to a 3d bose-einstein condensate. *Phys. Rev. Lett.* **113**, 215301 (2014).
34. Shah, R. et al. Probing the degree of coherence through the full 1d to 3d crossover. *Phys. Rev. Lett.* **130**, 123401 (2023).
35. Rydow, E. et al. Observation of a bilayer superfluid with interlayer coherence. *Nat. Commun.* **16**, 7201 (2025).
36. Jin, S. et al. Evidence of potts-nematic superfluidity in a hexagonal sp^2 optical lattice. *Phys. Rev. Lett.* **126**, 035301 (2021).
37. Greiner, M., Mandel, O., Esslinger, T., Hänsch, T. W. & Bloch, I. Quantum phase transition from a superfluid to a Mott insulator in a gas of ultracold atoms. *Nature* **415**, 39–44 (2002).

38. Plisson, T. et al. Coherence properties of a two-dimensional trapped Bose gas around the superfluid transition. *Phys. Rev. A* **84**, 061606 (2011).
39. Kato, Y., Zhou, Q., Kawashima, N. & Trivedi, N. Sharp peaks in the momentum distribution of bosons in optical lattices in the normal state. *Nat. Phys.* **4**, 617–621 (2008).
40. DeMarco, B., Lannert, C., Vishveshwara, S. & Wei, T.-C. Structure and stability of Mott-insulator shells of bosons trapped in an optical lattice. *Phys. Rev. A* **71**, 063601 (2005).
41. Yao, H., Giamarchi, T. & Sanchez-Palencia, L. Lieb-Liniger bosons in a shallow quasiperiodic potential: Bose glass phase and fractal Mott lobes. *Phys. Rev. Lett.* **125**, 060401 (2020).
42. Pitaevskii, L., Stringari, S. *Bose-Einstein Condensation* (Clarendon Press, 2003).
43. Anderson, M. H., Ensher, J. R., Matthews, M. R., Wieman, C. E. & Cornell, E. A. Observation of Bose-Einstein Condensation in a dilute atomic vapor. *Science* **269**, 198–201 (1995).
44. Prokof'ev, N., Ruebenacker, O. & Svistunov, B. Critical point of a weakly interacting two-dimensional Bose gas. *Phys. Rev. Lett.* **87**, 270402 (2001).
45. Pilati, S., Giorgini, S. & Prokof'ev, N. Critical temperature of interacting Bose gases in two and three dimensions. *Phys. Rev. Lett.* **100**, 140405 (2008).
46. Del Maestro, A. & Affleck, I. Interacting bosons in one dimension and the applicability of Luttinger-liquid theory as revealed by path-integral quantum Monte Carlo calculations. *Phys. Rev. B* **82**, 060515 (2010).
47. Gerbier, F. Boson Mott insulators at finite temperatures. *Phys. Rev. Lett.* **99**, 120405 (2007).
48. Boninsegni, M., Prokof'ev, N. & Svistunov, B. Worm algorithm for continuous-space path integral Monte Carlo simulations. *Phys. Rev. Lett.* **96**, 070601 (2006).
49. Boninsegni, M., Prokof'ev, N. V. & Svistunov, B. V. Worm algorithm and diagrammatic Monte Carlo: a new approach to continuous-space path integral Monte Carlo simulations. *Phys. Rev. E* **74**, 036701 (2006).
50. Troyer, M., Ammon, B. & Heeb, E. Parallel object oriented Monte Carlo simulations. In *Computing in Object-Oriented Parallel Environments* (eds, Caromel, D., Oldehoeft, R. R. & Tholburn, M.) 191–198 (Springer Berlin Heidelberg, 1998).
51. Albuquerque, A. et al. The Alps project release 1.3: open-source software for strongly correlated systems. *J. Magn. Magn. Mater.* **310**, 1187–1193 (2007).
52. Bauer, B. et al. The Alps project release 2.0: open source software for strongly correlated systems. *J. Stat. Mech.: Theory Exp.* **2011**, P05001 (2011).
53. Probing universal phase diagram of dimensional crossover with an atomic quantum simulator. Data set. *Zenodo* https://doi.org/10.5281/zenodo.17558857 (2025).

Acknowledgements

The authors thank Tianwei Zhou and Zekai Chen for their helpful discussions. This work is supported by the National Key Research and Development Program of China (Grants No. 2021YFA0718300 and No. 2021YFA1400900), National Natural Science Foundation of China (Grants No. 92365208) and The Fundamental Research Funds for the Central Universities, Peking University. This work is also supported by the Swiss National Science Foundation under grant number 200020-219400.

Author contributions

The work was conceived by J.T., H.Y., X.Z., T.G. and Z.Y. Experiments were performed by J.T., Z.Y and C.W. Data were analyzed by J.T. and J. L. Theoretical models and simulations were done by J.L., C.L., and L.P. Experiment preparations were done by Z.Y., C.W., and H.S. X.Z., H.Y. and T.G. supervised this work. H.Y., J.T., Z.Y., T.G., C.L. wrote the manuscript with input from all authors. All authors discussed the results.

Competing interests

The authors declare no competing interests.

Additional information

Supplementary information The online version contains supplementary material available at https://doi.org/10.1038/s41467-026-71881-3.

Correspondence and requests for materials should be addressed to Thierry Giamarchi, Hepeng Yao or Xiaoji Zhou.

Peer review information *Nature Communications* thanks the anonymous reviewer(s) for their contribution to the peer review of this work. A peer review file is available.